REVISTA DE LA UNIÓN MATEMÁTICA ARGENTINA
Vol. 64, No. 2, 2023, Pages 397–412
Published online: April 25, 2023
https://doi.org/10.33044/revuma.2893

A RICH AND COMPLEX DYNAMICS EMERGES BETWEEN THE SUBTHALAMIC NUCLEUS AND THE GLOBUS PALLIDUS EXTERNA IN THE BASAL GANGLIA

JULIÁN HURTADO-LÓPEZ, ANDRES FELIPE AMADOR-RODRIGUEZ, AND DAVID FERNANDO RAMIREZ-MORENO

Abstract. The oscillatory nature of basal ganglia activity is highly tied with some movement disorders. We study, through bifurcation analysis and computer simulations, the appearance of abnormal oscillations in an already proposed reduced neural circuit model of the subthalamic nucleus and globus pallidus loop. The results show that the model exhibits stable steady states associated to normal activity and oscillatory activity corresponding to the often termed "tremor frequency" oscillations due to their coherence with parkinsonian tremor observed in patients with Parkinson's disease.

1. Introduction

The basal ganglia (BG) constitute a neural network of diverse nuclei receiving projections from the cerebral cortex and projecting to the thalamus, which in turn projects to the neocortex, closing an essential circuit involved in a wide range of motor and cognitive functions. Understanding the wide range of functions carried out by the same structures with a well-known connectivity is a hard task, and it is even harder to explain them from a computational model that encompasses a complex dynamics. In addition, BG are involved in several neurological disorders such as Parkinson's and Huntington's diseases, as well as obsessive-compulsive disorders, schizophrenia, and addictions [6, 1]. An understanding of BG circuits [10] is indispensable in order to develop effective treatments for these disorders and explain the neural basis of motor control, habit-formation, decision-making, and reinforcement learning. Even though there is a significant amount of information about BG, researchers keep wondering how a single subcortical circuit supports a wide range of functions.

2020 *Mathematics Subject Classification.* 37N25, 37G35.

Key words and phrases. Bifurcation analysis, subthalamic nucleus, globus pallidus externa, oscillations, Parkinson's disease, delta band.

JHL and DFRM acknowledge the support of Universidad Autónoma de Occidente. AFAR acknowledges the support of Pontificia Universidad Javeriana Cali.

Actually, there are several computational models on BG but most of them focus on only one or two functions of the basal ganglia. One of the most widely used models was published by Gurney et al. [8, 9]. They formulated a BG model (called GPR model) in order to investigate the details of the operation of the BG disinhibition process, and it has been tested successfully as a mechanism of action selection of autonomous agents. A simple representative circuit composed of an ensemble of excitatory subthalamic nucleus (STN) neurons and an ensemble of inhibitory globus pallidus (GP) neuron interactions was analyzed by Gillies and Willshaw [7]. They showed that the two nuclei can be switched between states of high and low activity or can generate oscillations due to an appropriate external input. Holgado et al. [14] proposed a computational model of the STN-GPe network based on anatomical and electrophysiological studies. Their model intrinsically oscillates in the beta band (13–30 Hz), abnormal coherent oscillations, highly correlated with Parkinson's disease. In order to investigate the behavior when multiple interactive channels of globus pallidus pars externa (GPe) and subthalamic nucleus neurons are present, Merrison-Hort et al. [13] proposed and analyzed an extension of previous models. They performed a bifurcation analysis of an isolated channel model of the STN-GPe system where a rich variety of neural dynamics was exhibited. Recently, Chakravarthy and Balasubramani [3] presented a simple network model of BG called GEN (Go/Explore/NoGo) where the STN and GPe modules are modeled as an excitatory-inhibitory loop which is able to produce oscillations. In their work, the dynamics of the STN-GPe system is characterized as correlations of neural activity when different connectivity parameters are varied.

Understanding the interaction between the basal ganglia and other brain areas is essential for finding new treatments for disorders affecting the neural systems supporting motor and cognitive behaviors. Achieving a comprehensive computational model of BG will further the development of theoretical neurobiology. There will be important contributions to different fields, such as computer science, applied mathematics, robotics, and machine learning.

In this paper we will study a mean firing rate mathematical model of a coupled pair of STN and GPe populations based on the GEN model [3]. The goal of this study is to investigate how changes in network parameters can lead to different dynamical modes such as steady, oscillatory, or bistable behaviors as well as to analyze the presence of oscillations associated with Parkinson's disease. Specifically, we perform a bifurcation analysis of a network of two simplified neurons to investigate different dynamical modes with respect to changes in inputs and interconnection strengths.

2. Models and methods

2.1. **The GPe-STN loop model.** The model we propose is based on a model of leaky-integrator neurons, which were used in the GEN model [3]. The GPe-STN circuit is represented by two neurons which form a recurrent excitatory-inhibitory loop, as illustrated in Fig. 1, that exhibits a rich variety of neural dynamics.

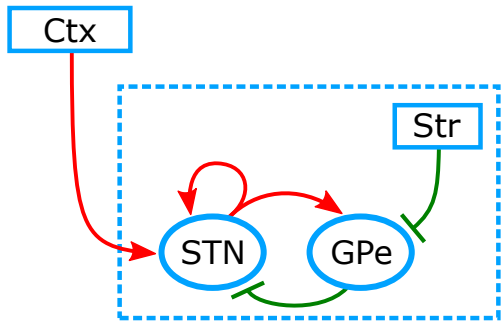

FIGURE 1. Schematic diagram of the interactions between and within the STN and GPe. Lines ending in a bar are inhibitory (GABAergic) synapses and those ending in arrows are excitatory (glutamatergic) synapses.

The dynamics of a single STN-GPe neuron subpopulation pair is given as

$$\tau_s \frac{dx^{\mathrm{STN}}}{dt} = -x^{\mathrm{STN}} + w_{ss}U^{\mathrm{STN}} - w_{gs}x^{\mathrm{GPe}} + I^{\mathrm{HDP}} + K^{\mathrm{STN}}, \tag{2.1}$$

$$\tau_g \frac{dx^{\mathrm{GPe}}}{dt} = -x^{\mathrm{GPe}} + w_{sg}U^{\mathrm{STN}} - w_{gg}x^{\mathrm{GPe}} - I^{\mathrm{D2}}, \tag{2.2}$$

$$U^{\mathrm{STN}} = \tanh(\lambda^{\mathrm{STN}}x^{\mathrm{STN}}), \tag{2.3}$$

where the time-dependent variables x^{STN} and x^{GPe}, respectively, represent the average activity of all neurons of the excitatory STN subpopulation and inhibitory GPe subpopulation. τ_s and τ_g represent the average membrane time constants of neurons in the STN and GPe, respectively. The nonnegative connection strength parameters are wss, wsg, wgg, and wgs and represent the strength of synaptic connectivity between the populations, where w_{ij} is the connection strength from population i to population j. Finally, I^{HDP} is the constant level of cortical excitation of the STN (the hyperdirect pathway), I^{D2} represents a constant level of inhibition of the GPe coming from D2-expressing neurons of striatum (the indirect pathway), and K^{STN} is a constant bias current given to STN neurons. It is also worth mentioning that the output of the GPe subpopulation neurons is linear, that is, $U^{\mathrm{GPe}} = x^{\mathrm{GPe}}$.

For a simpler notation, let $x = x^{\mathrm{STN}}$, $y = x^{\mathrm{GPe}}$, $\lambda = \lambda^{\mathrm{STN}}$, and $I_2 = I^{\mathrm{D2}}$. Further, it is useful to let $I_1 = I^{\mathrm{HDP}} + K^{\mathrm{STN}}$ in order to reduce the number of parameters in the system. Taking into account these changes, the system (2.1)–(2.3) can be represented in matrix form as follows:

$$\begin{pmatrix} \dot{x} \\ \dot{y} \end{pmatrix} = \begin{pmatrix} \frac{1}{\tau_s}\left(-x + w_{ss}\tanh(\lambda x) - w_{gs}y + I_1\right) \\ \frac{1}{\tau_g}\left(-y + w_{sg}\tanh(\lambda x) - w_{gg}y - I_2\right) \end{pmatrix}. \tag{2.4}$$

In order to study the time-dependent dynamics and the steady state behavior of the neural network, it is quite important to analyze the equilibrium points of equation (2.4) and their stability properties.

2.1.1. *Equilibria and stability.* Given the autonomous system in (2.4), the x and y nullclines are respectively

$$y = \frac{1}{w_{gs}}\left(-x + w_{ss}\tanh(\lambda x) + I_1\right),$$
$$y = \frac{1}{1+w_{gg}}\left(w_{sg}\tanh(\lambda x) - I_2\right).$$

These nullclines give rise to system's equilibria by solving the following nonlinear system:

$$\begin{aligned}(1+w_{gg})x + (w_{\rm gs}w_{\rm sg} - (1+w_{\rm gg})w_{\rm ss})\tanh(\lambda x) - (1+w_{\rm gg})I_1 - w_{gs}I_2 = 0,\\ (1+w_{gg})y - w_{sg}\tanh(\lambda x) + I_2 = 0.\end{aligned}$$

Remark 2.1. The Jacobian matrix for the right-hand side of equation (2.4) around (x, y) is

$$J(x,y) = \begin{pmatrix} -\dfrac{1}{\tau_s}\left(1 - \lambda w_{ss}\operatorname{sech}^2(\lambda x)\right) & -\dfrac{w_{gs}}{\tau_s} \\ \dfrac{\lambda w_{sg}}{\tau_g}\operatorname{sech}^2(\lambda x) & -\dfrac{1+w_{\rm gg}}{\tau_g} \end{pmatrix}.$$

The trace and the determinant of $J(x, y)$ are respectively given by

$$\operatorname{Tr}(J) = -\frac{(1+w_{\rm gg})\tau_s + \tau_g}{\tau_s\tau_g} + \frac{\lambda w_{\rm ss}}{\tau_s}\operatorname{sech}^2(\lambda x)$$

and

$$\det(J) = \frac{1+w_{\rm gg}}{\tau_s\tau_g} + \frac{\lambda(w_{\rm gs}w_{\rm sg} - (1+w_{\rm gg})w_{\rm ss})}{\tau_s\tau_g}\operatorname{sech}^2(\lambda x).$$

Proposition 2.2. *Consider the system given by* (2.4) *with* $w_{gs}w_{sg} - (1+w_{gg})w_{ss} = 0$. *The following statements hold.*

(1) $(x^*, y^*) \in \mathbb{R}^2$ *is an equilibrium point of the system* (2.4) *if and only if*

$$x^* = I_1 + \frac{w_{ss}}{w_{sg}}I_2 \quad \textit{and} \quad y^* = \frac{w_{ss}}{w_{gs}}\tanh\left(\lambda\left(I_1 + \frac{w_{ss}}{w_{sg}}I_2\right)\right) - \frac{w_{ss}}{w_{gs}w_{sg}}I_2. \tag{2.5}$$

(2) *The sets*

$$H_c^1 = \left\{(I_1, I_2) : I_1 + \frac{w_{ss}}{w_{sg}}I_2 = \frac{1}{\lambda}\operatorname{arctanh}\left(\sqrt{1 - \frac{\tau_g w_{ss} + w_{gs}w_{sg}\tau_s}{\tau_g w_{ss}^2\lambda}}\right)\right\}, \tag{2.6}$$

$$H_c^2 = \left\{(I_1, I_2) : I_1 + \frac{w_{ss}}{w_{sg}}I_2 = \frac{1}{\lambda}\operatorname{arctanh}\left(-\sqrt{1 - \frac{\tau_g w_{ss} + w_{gs}w_{sg}\tau_s}{\tau_g w_{ss}^2\lambda}}\right)\right\}, \tag{2.7}$$

are bifurcation sets, at the (I_1-I_2) *parameter space, corresponding with an Andronov–Hopf bifurcation of codimension one.*

(3) *The set*

$$H_c^3 = \left\{ (\tau_s, \tau_g) : \tau_s = \frac{w_{ss}}{w_{gs} w_{sg}} \left(w_{ss} \lambda \operatorname{sech}^2 \left(\lambda \left(I_1 + \frac{w_{ss}}{w_{sg}} I_2 \right) \right) - 1 \right) \tau_g \right\}$$

is a bifurcation set, at the (τ_s-τ_g) parameter space, corresponding with an Andronov–Hopf bifurcation of codimension one.

Proof. (1) It is sufficient to consider $F_i = \mathbf{0}$, where the vector fields F_i are the components of the right-hand side defined in (2.4) and $\mathbf{0}$ is the null vector.

(2)-(3) It is sufficient to consider $\operatorname{Tr}(J) = 0$. □

Remark 2.3. It is easy to conclude that at the 2-parameter space, curves corresponding with an Andronov–Hopf bifurcation are straight lines, as shown in Fig. 4a.

2.2. **The GEN model.** Chakravarthy and Balasubramani [3] modeled and analyzed the STN-GPe system based on the parameters defined in Table 1. They demonstrated the emergence of the Explore regime. The exploratory dynamics is necessary for reward-based or reinforcement learning and the authors concluded that oscillations of the STN-GPe system drive exploratory behavior. The GEN model is also involved in binary action selection; however, due to the complex dynamics of the STN-GPe system, they proved that it is not necessary for the winning action to be always the one represented with greater saliency and proposed three possible outcomes [2]: "Go" (winning neuron has greater salience), "Explore" (winning neuron has lesser salience), and "NoGo" (no winner and therefore no action selection). These regimes were controlled by dopamine in a scalable manner, i.e., the Go regime is exhibited with high probability for large values of dopamine, the Explore regime is also selected with the probability maximized for moderate values of dopamine, and the NoGo for the smallest values.

TABLE 1. Fixed parameter values taken from [3].

Parameters	Symbol	Value
Self-excitation within the STN	w_{ss}	1
Coupling strength within GPe subpopulation	w_{gg}	0
Connection strength from STN to GPe	w_{sg}	1
Connection strength from GPe to STN	w_{gs}	1
Time constant of neurons in the STN	τ_s	0.03
Time constant of neurons in the GPe	τ_g	0.1
Constant bias current given to STN neuron	K^{STN}	-1
Slope parameter of the sigmoid function	λ^{STN}	3

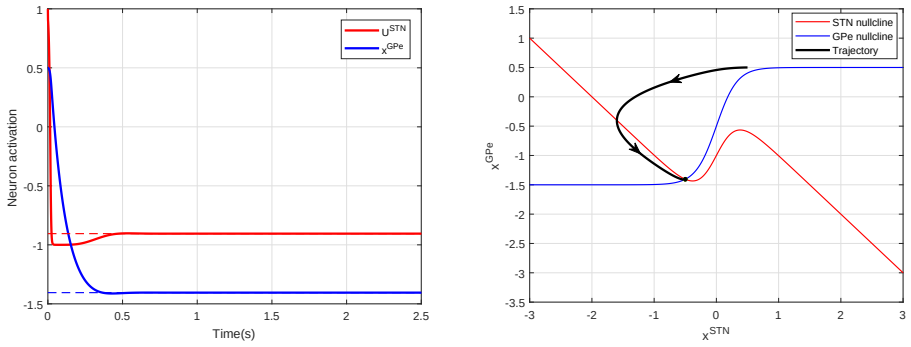

(a) (b)

FIGURE 2. Steady-state regime when $I^{\mathrm{HDP}} = 0$ and $I^{\mathrm{D2}} = 0.5$. (a) Neural activation and (b) phase portrait showing a stable fixed point.

2.2.1. *Simulating the GPe-STN loop model.* Let us consider the system (2.1)–(2.3) based on the parameter values from Table 1 along with $I^{\mathrm{HDP}} = 0$ and $I^{\mathrm{D2}} = 0.5$. Under these specific conditions, the STN-GPe circuit shows a single stable steady-state or stable fixed point (Fig. 2a) and it is represented by the intersection of the x^{STN}- and x^{GPe}-nullclines as shown in Fig. 2b.

Note that the system with this set of parameters satisfies the hypothesis of Proposition 2.2. Then, from equation (2.5), $(x^*, y^*) = (-0.5, -1.4051)$ is the stable equilibrium point, analytically obtained and exhibited in Fig. 2. The stability of the equilibrium point is due to the Jacobian matrix at the equilibrium point having negative trace and positive determinant (the Jacobian matrix, its trace, and its determinant were defined in Remark 2.1).

When considering the value of the parameter I^{D2} as 0.9, the system changes from a single steady-state regime to a globally stable limit cycle (oscillatory regime) as shown in Fig. 3. The limit cycle is the closed trajectory in phase space that contains within its interior an unstable stationary point of the system as shown in Fig. 3b. The emergence of this limit cycle means that globally stable oscillations are possible in the STN-GPe circuit (Fig. 3a) by increased striatal input (I^{D2}) to GPe. These results were presented in [3] and corroborated by electrophysiological data [5].

2.2.2. *Bifurcation under one and two parameter variation.* Finding the exact value of I^{D2} where the system generates a limit cycle would be a significant result. However, we found a large area of the state space where the system exhibits oscillatory behavior. This result is presented in Fig. 4 and derived from Proposition 2.2(2). Fig. 4a shows a 2D bifurcation diagram of the STN-GPe system for fixed parameter values presented in Table 1 while parameters I^{D2} and I^{HDP} are varied. The 2D bifurcation diagram represents the $(I^{\mathrm{D2}}, I^{\mathrm{HDP}})$ parameter space which is divided

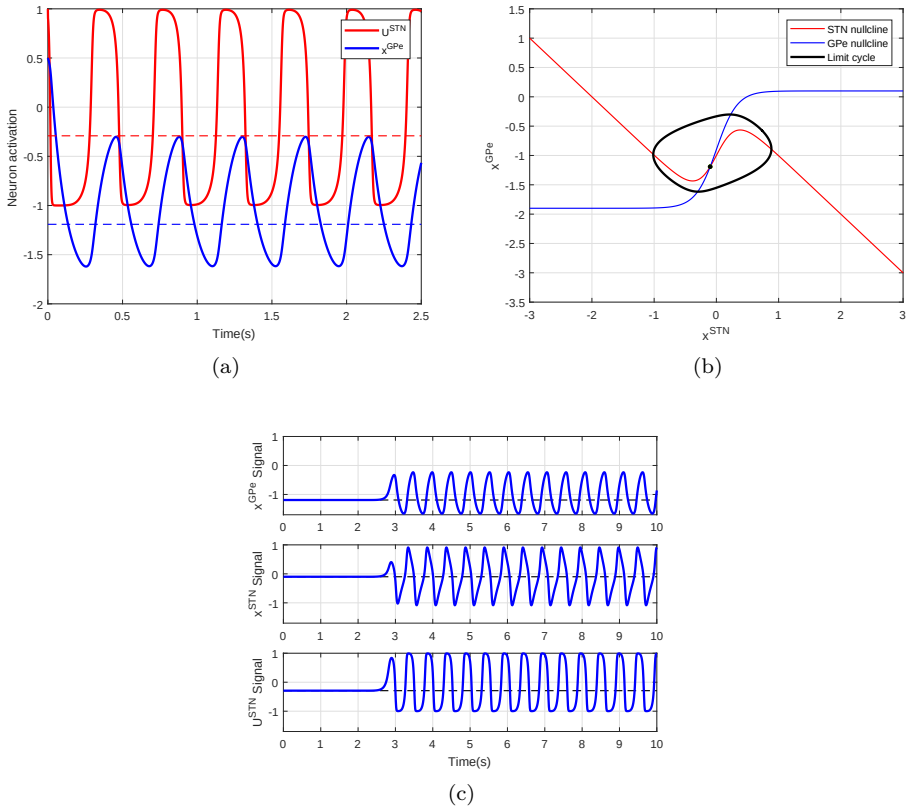

FIGURE 3. Oscillatory regime when $I^{\mathrm{HDP}} = 0$ and $I^{\mathrm{D2}} = 0.9$. (a) Neural activation and (b) phase portrait showing a limit cycle. (c) The activity signal of the system when it is started near to the unstable equilibrium point.

in five regions, by four straight lines. From Fig. 4a, the two continuous black lines are obtained from equations (2.6)–(2.7) as defined in Proposition 2.2 and their equations are $I^{\mathrm{D2}} = -I^{\mathrm{HDP}} + 1 + \frac{1}{3}\operatorname{arctanh}\left(\pm\sqrt{\frac{17}{30}}\right)$. Specifically, every point on the line indicates the values of I^{D2} and I^{HDP} where there occurs a subcritical Andronov–Hopf (A–H) bifurcation. A subcritical A–H bifurcation leads to the presence of an unstable limit cycle. The other two continuous dashed lines give place to a limit point bifurcation of cycles (LPC). They were obtained with the MATCONT package, which performs numerical continuation of equilibria [4]. The LPC bifurcation is a type of saddle-node bifurcation of limit cycles, in which a stable limit cycle is approached by an unstable one, they coalesce, and then they disappear.

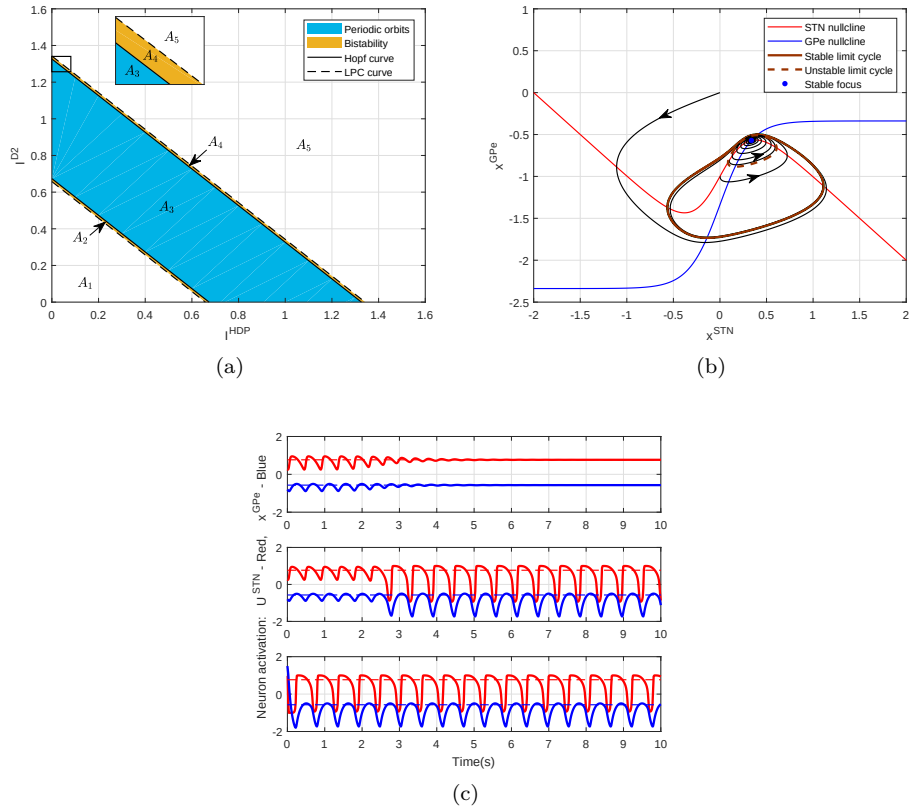

FIGURE 4. (a) 2D bifurcation diagram showing the Hopf bifurcation curves that the STN-GPe system undergoes under variation of I^{D2} and I^{HDP}. (b) Phase portrait with $I^{\mathrm{HDP}} = 0$ and $I^{\mathrm{D2}} = 1.3381$ showing three different trajectories whose time series, depending on initial conditions, are shown in (c).

In Fig. 4a, within each of the regions A_1, A_2, ..., A_5, the phase portraits of the system are topologically equivalent. Within regions A_1 and A_5 the system has only steady-state behavior: a "normal regime" represented by a single, stable, equilibrium point. On the other hand, within region A_3 the dynamical system generates an oscillatory regime due to a stable limit cycle, surrounding an unstable spiral, which is a global attractor. This region is limited by the two subcritical A–H bifurcation curves. Fig. 4b shows an example of the phase portrait that is representative of the system's behaviour in region A_3. The time series in Fig. 4c show the activity signal of the system when it is started near to the unstable equilibrium point. Since it is unstable, it repels nearby trajectories and, consequently, trajectories are attracted by the stable limit cycle. Finally, the most interesting

behavior is found within regions A_2 and A_4. Within these regions the system has a bistability regime between steady-state and oscillatory behavior that depends on initial conditions. The region A_2 is bounded at the top by a subcritical A–H bifurcation curve and at the bottom by an LPC bifurcation curve. Similarly, the region A_4 is bounded above by an LPC bifurcation curve and below by a subcritical A–H bifurcation curve. The last two regions are exhibited in the one-dimensional bifurcation diagram shown in Fig. 5a.

An example of a phase portrait, when $I^{\mathrm{HDP}} = 0$ and $I^{\mathrm{D2}} = 1.3381$, that represents the behavior of the system in region A_4 is shown in Fig. 4b. This figure shows the nullclines with an intersection at the stable spiral, the stable and unstable limit cycles, and three trajectories starting from different initial conditions. Bistability within this region leads to the fact that both the fixed point and the stable limit cycle have local basins of attraction. In fact, the basin of attraction of the attracting fixed point is the open set inside the unstable limit cycle (dashed brown line). Therefore, trajectories starting from this set tend to the fixed point as shown in Fig. 4b. The time series at the top panel in Fig. 4c show the activity signal of the system when it is started near to the unstable limit cycle. Since the limit cycle is unstable, it repels nearby trajectories and, consequently, trajectories are attracted by the stable equilibrium.

On the other hand, the region inside the stable limit cycle (continuous brown line) is divided by the unstable limit cycle into two concentric areas. Trajectories that start within the outer area tend to the stable cycle as shown in Fig. 4b. In the middle panel in Fig. 4c, the time series show the activity signal of the system when it is started near to the unstable limit cycle. Once again, as the limit cycle is unstable, it repels nearby trajectories and, consequently, trajectories are attracted by the stable limit cycle. Finally, the entire basin of attraction of the stable limit cycle is completed by the region outside of it (see Fig. 4b). The time series at the bottom panel in Fig. 4c show the activity signal corresponding with initial conditions outside of the stable limit cycle. The last two time series show that the system exhibits an oscillatory regime. To sum up, the system's behavior within regions A_2 and A_4 is bi-stable and, depending on initial conditions, may show either steady-state or oscillatory activity regimes.

In our simulations, we performed a one-dimensional bifurcation analysis in order to have a better visualization of the dynamical repertoire of the STN-GPe system undergoing a parameter variation. A bifurcation diagram may reveal critical values and qualitative changes that separate the different dynamical behaviors.

For example, a numerical continuation was performed by starting at a fixed point and varying the parameter I^{D2} from 0.5 to 1.5 and keeping I^{HDP} fixed at 0. Simulation results were plotted, as bifurcation diagrams, in Fig. 5. Fig. 5a depicts, in detail for x^{STN}, qualitative changes and different regimes when I^{D2} varies from 0.5 to 1.5. These nonlinear phenomena occur, at the same values, for U^{STN} (Fig. 5b) and x^{GPe} (Fig. 5c).

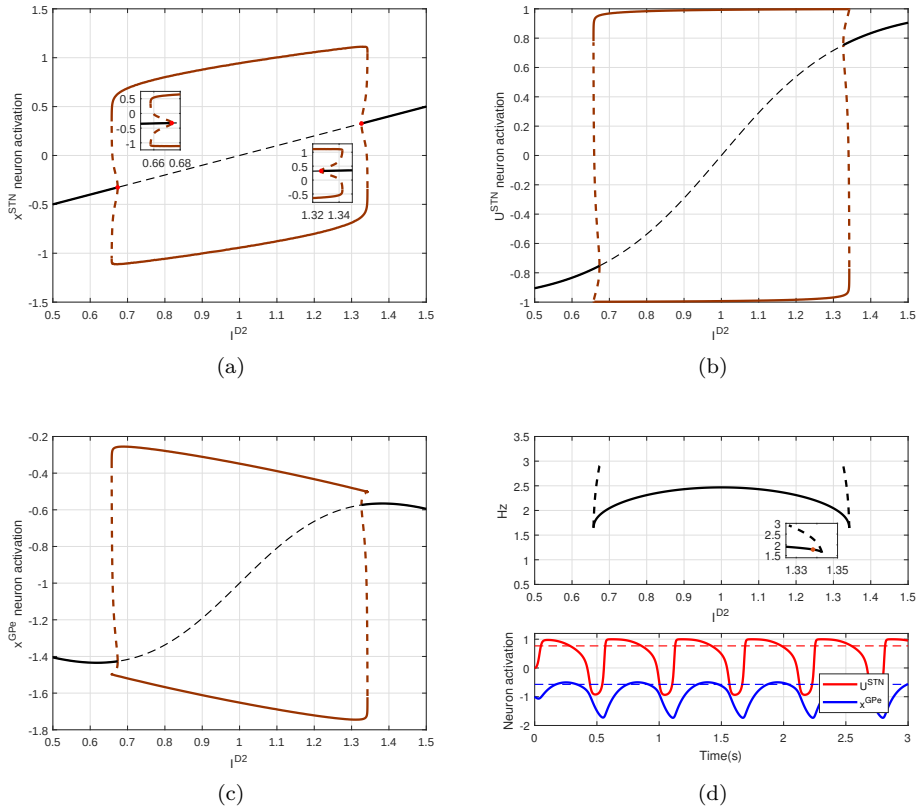

FIGURE 5. (a)–(c) The effect of I^{D2} on the generation of oscillations with $I^{HDP} = 0$. (d) Top: frequency range 0.5–4 Hz (delta band); bottom: oscillatory activity of the model with $I^{D2} = 1.338$.

Figs. 5a–5c show that the STN-GPe system presents a steady-state regime when $I^{D2} < 0.6575$. At $I^{D2} = 0.6575$ the STN-GPe system undergoes an LPC bifurcation, a limit cycle that is neither stable nor unstable. As I^{D2} increases, this limit cycle bifurcates into a stable limit cycle and an unstable one giving rise to a bistable regime. It should be noted that the equilibrium point remains stable. The bistable regime is maintained until a small unstable limit cycle shrinks to the stable equilibrium and makes it lose stability. At this bifurcation point, amplitude of the limit cycle becomes zero and then a subcritical Andronov–Hopf bifurcation emerges. The A–H bifurcation occurs at $I^{D2} = 0.6735$, where a pair of purely imaginary complex conjugate eigenvalues is reached, and a positive *first Lyapunov coefficient* also appears, $l_1 = 98.19735$.

Another subcritical A–H bifurcation occurs at $I^{\mathrm{D2}} = 1.3264$. Indeed, there are two eigenvalues of the equilibrium where the real part becomes zero and then positive, meaning that the equilibrium (focus) is no longer unstable, while the first Lyapunov coefficient is positive, $l_1 = 98.19747$. Thus, there should exist an unstable limit cycle bifurcating from the equilibrium, located at $(x^{\mathrm{STN}}, x^{\mathrm{GPe}}) = (0.326441, -0.573668)$. This means that a new bistable regime takes place until the stable and the unstable limit cycles approach, coalesce and then annihilate each other, thus the STN-GPe system, once again, undergoes an LPC bifurcation at $I^{\mathrm{D2}} = 1.3425$. Ultimately, the STN-GPe system presents a steady-state regime when $I^{\mathrm{D2}} > 1.3425$.

In order to find, from the model, indications of the presence of oscillations associated with Parkinson's disease, we plotted a diagram (the one at the top in Fig. 5d) that shows the frequency presented between the values of I^{D2} where the oscillations occur. The diagram shows that the frequency of the sustained oscillation is in the range 1.7–2.5 Hz when I^{D2} takes values in the interval $(0.6575, 1.3425)$. It can be seen from the graph that those frequencies are related with stable oscillations whereas unstable oscillations (dashed lines) may reach frequencies up to 2.9 Hz. At the bottom of Fig. 5d the oscillatory activity of the coupled nucleus model with $I^{\mathrm{D2}} = 1.338$ is shown. Accordingly, it falls into the delta band (0.5–4 Hz). The delta frequency band shows oscillatory activity within the basal ganglia in patients with Parkinson's disease in relation to tremor, but their relation to other parkinsonian symptoms is not well known yet [15]. This low-frequency oscillations band has been subject to very limited study, and little has been reported on functions related to it. probably because the delta band is particularly susceptible to movement artifacts and is often filtered. This oscillation can be detected, from EEG studies, during slow wave sleep and cognitive task execution [16].

When the model was simulated varying parameter values corresponding to the slope parameter of the sigmoid function (λ^{STN}) and connections strength, w_{sg} and w_{gs}, and keeping I^{D2} fixed at 0.7, the STN-GPe system also produces oscillations.

Similar to the previous diagrams, Figs. 6a-6b show that the STN-GPe system presents an oscillatory regime and Figs. 6c-6d show the frequency of the sustained oscillations in the range 1.25–2.9 Hz.

In Fig. 6a, the oscillatory regime is present when λ^{STN} takes values in the interval $(1.642, 4.114)$. This interval is determined due to the STN-GPe system undergoing, first, a subcritical Andronov–Hopf bifurcation and then an LPC bifurcation. At $\lambda^{\mathrm{STN}} = 3.728$ a subcritical Andronov–Hopf bifurcation emerges and then a new bistable regime takes place.

When changing the value of I^{D2} to 0.657, the oscillatory regime emerges when λ^{STN} is in the interval $(2.052, 2.985)$, as illustrated in Fig. 6b. This range is determined due to the fact that the STN-GPe system undergoes two LPC bifurcations. The diagram also shows, at $\lambda^{\mathrm{STN}} = 2.096$ and $\lambda^{\mathrm{STN}} = 2.41$, two subcritical Andronov–Hopf bifurcations, which define two bistable regimes for the system. Notice that there is a wide range of lambda values where the system is bistable. Regarding the frequency of the system for both I^{D2} values, oscillatory conditions

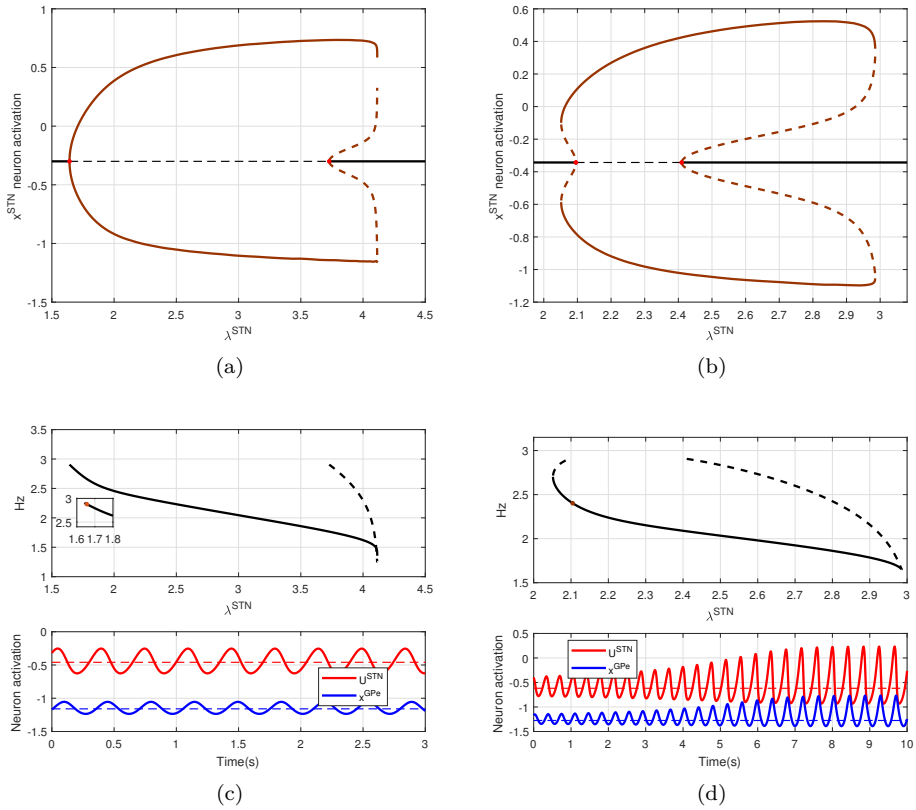

FIGURE 6. The effect of λ^{STN} on the generation of oscillations with $I^{\mathrm{HDP}} = 0$ and (a) $I^{\mathrm{D2}} = 0.7$, (b) $I^{\mathrm{D2}} = 0.657$. (c) Top: frequency range 0.5–4 Hz (delta band); bottom: oscillatory activity of the model with $\lambda^{\mathrm{STN}} = 1.6555$. (d) Top: frequency range 0.5–4 Hz (delta band); bottom: oscillatory activity of the model with $\lambda^{\mathrm{STN}} = 2.104$.

mainly fall in the range of 1–3 Hz, which is the same parkinsonian oscillation delta band mentioned before, as shown at the top of Figs. 6c and 6d.

As a last attempt to find high-frequency oscillations, the values of I^{D2} and λ^{STN} were set at 0.9 and 3, respectively, and the values of the connections strength w_{sg} and w_{gs} were varied. A 2D bifurcation diagram of the STN-GPe system is shown in Fig. 7a. The equilibria that correspond to the system solution are shown as solid blue and green lines, the blue lines represent LP (limit point) bifurcations (or saddle-node bifurcations) and the green lines represent Andronov–Hopf bifurcations. The latter are responsible for oscillations occurring in the system as seen before.

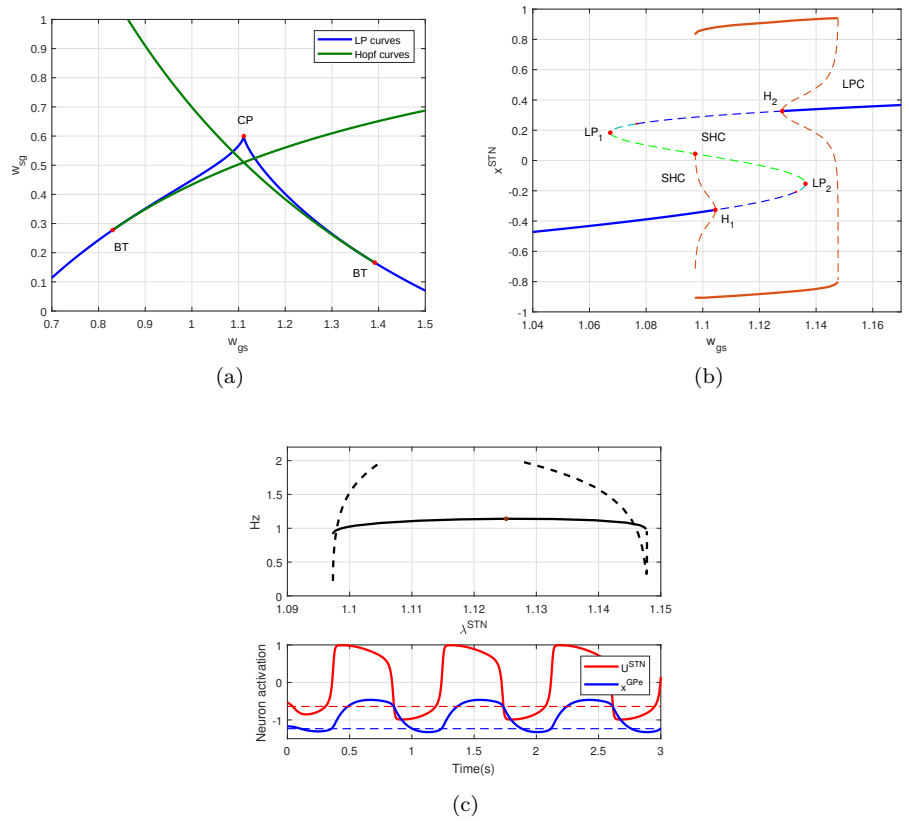

FIGURE 7. (a) (w_{sg}, w_{gs}) parameter bifurcation diagram showing Andronov–Hopf (green lines) and limit point (blue lines) bifurcation curves that give rise to codimension-two bifurcations such as CP (cusp point) and BT (Bogdanov–Takens), with $I^{\mathrm{HDP}} = 0$ and $I^{\mathrm{D2}} = 0.9$. (b) The effect of w_{gs} on the generation of oscillations with $w_{sg} = 0.52$. (c) Top: frequency range 0.5–4 Hz (delta band); bottom: oscillatory activity of the model with $w_{gs} = 1.125$.

Similarly to that seen in Fig. 4a, these curves separate the (w_{sg}, w_{gs}) parameter space into different regions in which the phase portraits of the STN-GPe system are topologically equivalent. On the other hand, Fig. 7a shows the presence of codimension-two bifurcations such as cusp point (CP) and Bogdanov–Takens (BT) as well. The occurrence of a CP bifurcation is due to the fact that two branches of the limit point bifurcation curve meet tangentially. The cusp bifurcation strongly suggests the existence of a hysteresis phenomenon [12]. BT bifurcation points are those at which Andronov–Hopf curves terminate on saddle-node curves. A

BT bifurcation gives rise to an LPC bifurcation, specifically, the emergence of a homoclinic orbit (HC), for nearby parameter values [12].

Fig. 7b, for example, displays all bifurcations found for the system equilibria in the case $w_{sg} = 0.52$. The figure shows two subcritical Hopf bifurcations H_1 and H_2 that occur where the parameter $w_{gs} = 1.104$ or $w_{gs} = 1.128$. From H_2, as w_{gs} increases, the two limit cycles disappear at $w_{gs} = 1.148$, where the STN-GPe system undergoes an LPC bifurcation. From H_1, as w_{gs} decreases, the two limit cycles disappear at $w_{gs} = 1.097$, where the STN-GPe system undergoes an SHC (saddle-homoclinic orbit) bifurcation [11]. The SHC bifurcation corresponds to a limit cycle that grows into a saddle point; the unstable manifold of the saddle makes a loop and returns via the stable manifold. As mentioned before, in the graph of Fig. 7b a kind of hysteresis phenomena can be recognized when considering different values of w_{gs}. If it is varied slowly back and forth, the connection strength w_{gs} between a value where the A–H bifurcations occur and another one after LPC occur, it can be noticed that the system promotes a transition from an oscillatory regime to a normal one. Once a normal regime is elicited, reducing the connection strength no longer evokes an oscillatory regime, but simply promotes a normal regime. Finally, Fig. 7b also shows two limit points LP_1 and LP_2 where unstable equilibria disappears or appears depending on the direction of movement of the bifurcation parameter.

Regarding the frequency of the system, oscillatory conditions mainly fall in the range of 1–3 Hz, and again a low-frequency band was found as shown at the top of Fig. 7c. At the bottom of Fig. 7c the oscillatory activity of the STN-GPe system with $w_{gs} = 1.125$ is shown.

3. Conclusions

The connectivity and interaction between the nuclei that make up the BG and, in particular, the excitatory-inhibitory loop between STN and GPe, produce a rich and diverse dynamics in this system, with the presence of stable and unstable states, oscillatory regimes of diverse nature, transitions between them and bifurcation points, among others. The strong dependence of the dynamics exhibited on the system parameters was shown in detail in the previous section.

From a functional neuro-anatomical perspective, BG are involved not only in motor control tasks, but also in cognitive processes such as decision-making in exploratory or exploitative modes, or transitions between them, shown by the subjects in response to their own needs or to demands of their environment.

The dynamics described in this work is a more detailed theoretical framework for the explanation of the behaviors mentioned above. The identification of variations in the values of specific parameters of the mathematical model as a source and explanation of oscillatory regimes, of stable or unstable states and of observed transitions, allows us to point out to correlations between organic elements in BG and elements of the mathematical model, in addition to the correlations formulated between regimes or states of the model and behaviors of the subject. Such is the

case with the neurotransmitter dopamine and the ionic currents that ensure phasic or basal states that find their correlates in the model.

The appearance of oscillations in the proposed model, which may correspond to pathological states of sporadic or constant tremors such as those that occur in Parkinson's disease, shows the scope of the mathematical model in achieving a faithful representation of the physiology of BG and its neural functionality. In a more detailed and complete exploration of the structure and dynamics of BG in the near future, from the approach of the nonlinear dynamics of complex systems, a significant contribution can be expected to theoretical neurobiology and therapeutic neuro-pharmacology in the treatment of diseases of a dynamic nature.

References

[1] D. Belin and B. J. Everitt, Drug addiction: The neural and psychological basis of a compulsive incentive habit, in *Handbook of Basal Ganglia Structure and Function*, 571–592, Handbook of Behavioral Neuroscience, 20, Elsevier, 2010.

[2] V. S. Chakravarthy and P. P. Balasubramani, Basal ganglia system as an engine for exploration, in *Encyclopedia of Computational Neuroscience*, 315–327, Springer New York, 2015, https://doi.org/10.1007/978-1-4614-7320-6_81-1.

[3] V. S. Chakravarthy and P. P. Balasubramani, The basal ganglia system as an engine for exploration, in *Computational Neuroscience Models of the Basal Ganglia*, 59–96, Springer Singapore, 2018, https://doi.org/10.1007/978-981-10-8494-2_5.

[4] A. Dhooge, W. Govaerts, and Yu. A. Kuznetsov, MATCONT: a MATLAB package for numerical bifurcation analysis of ODEs, *ACM Trans. Math. Software* **29** (2003), no. 2, 141–164. MR 2000880.

[5] J. Flores-Hernández, C. Cepeda, E. Hernández-Echeagaray, C. R. Calvert, E. S. Jokel, A. A. Fienberg, P. Greengard, and M. S. Levine, Dopamine enhancement of NMDA currents in dissociated medium-sized striatal neurons: Role of D1 receptors and DARPP-32, *J. Neurophysiol.* **88** (2002), no. 6, 3010–3020, PMID: 12466426, https://doi.org/10.1152/jn.00361.2002.

[6] A. Galvan, A. Devergnas, and T. Wichmann, Alterations in neuronal activity in basal ganglia-thalamocortical circuits in the parkinsonian state, *Front. Neuroanat.* **9** (2015), 5, https://doi.org/10.3389/fnana.2015.00005.

[7] A. Gillies, D. Willshaw, and Z. Li, Subthalamic pallidal interactions are critical in determining normal and abnormal functioning of the basal ganglia, *Proc. R. Soc. Lond. B* **269** (2002), 545–551, https://doi.org/10.1098/rspb.2001.1817.

[8] K. Gurney, T. J. Prescott, and P. Redgrave, A computational model of action selection in the basal ganglia. I. A new functional anatomy, *Biol. Cybern.* **84** (2001), no. 6, 401–410, https://doi.org/10.1007/PL00007984.

[9] K. Gurney, T. J. Prescott, and P. Redgrave, A computational model of action selection in the basal ganglia. II. Analysis and simulation of behaviour, *Biol. Cybern.* **84** (2001), no. 6, 411–423, https://doi.org/10.1007/PL00007985.

[10] E. J. Hwang, The basal ganglia, the ideal machinery for the cost-benefit analysis of action plans, *Front. Neural Circuits* **7** (2013), Art. 121, 6 pp. https://doi.org/10.3389/fncir.2013.00121.

[11] E. M. Izhikevich, Neural excitability, spiking and bursting, *Internat. J. Bifur. Chaos Appl. Sci. Engrg.* **10** (2000), no. 6, 1171–1266. MR 1779667.

[12] Y. A. Kuznetsov, *Elements of Applied Bifurcation Theory*, third edition, Applied Mathematical Sciences, 112, Springer-Verlag, New York, 2004. MR 2071006.

[13] R. Merrison-Hort, N. Yousif, F. Njap, U. G. Hofmann, O. Burylko, and R. Borisyuk, An interactive channel model of the basal ganglia: bifurcation analysis under healthy and Parkinsonian conditions, *J. Math. Neurosci.* **3** (2013), Art. 14, 29 pp. MR 3338740.

[14] A. J. Nevado Holgado, J. R. Terry, and R. Bogacz, Conditions for the generation of beta oscillations in the subthalamic nucleus–globus pallidus network, *J. Neurosci.* **30** (2010), no. 37, 12340–12352, https://doi.org/10.1523/JNEUROSCI.0817-10.2010.
[15] T. C. Whalen, A. M. Willard, J. E. Rubin, and A. H. Gittis, Delta oscillations are a robust biomarker of dopamine depletion severity and motor dysfunction in awake mice, *J. Neurophysiol.* **124** (2020), no. 2, 312–329, PMID: 32579421, https://doi.org/10.1152/jn.00158.2020.
[16] Z. Yin, G. Zhu, B. Zhao, Y. Bai, Y. Jiang, W.-J. Neumann, A. A. Kühn, and J. Zhang, Local field potentials in Parkinson's disease: A frequency-based review, *Neurobiol. Dis.* **155** (2021), 105372, 10 pp., https://doi.org/10.1016/j.nbd.2021.105372.

Julián Hurtado-López✉
Departamento de Matemáticas y Estadística, Universidad Autónoma de Occidente, Cali, Colombia
jhurtado@uao.edu.co

Andres Felipe Amador-Rodriguez
Departamento de Ciencias Naturales y Matemáticas, Pontificia Universidad Javeriana, Cali, Colombia
afamador@javerianacali.edu.co

David Fernando Ramirez-Moreno
Departamento de Física, Universidad Autónoma de Occidente, Cali, Colombia
dramirez@uao.edu.co

Received: September 29, 2021
Accepted: March 17, 2022